ACS APPLIED ELECTRONIC MATERIALS

pubs.acs.org/acsaelm

Article

m-Line Frank–Shockley Partial Dislocations in Wurtzite GaN: Atomistic Calculations and High Resolution Electron Microscopy Imaging

Imad Belabbas, Joanna Moneta, George P. Dimitrakopulos, Joseph Kioseoglou, Jun Chen, Witold Chromiński, and Julita Smalc-Koziorowska*

Cite This: https://doi.org/10.1021/acsaelm.5c00859

Read Online

ABSTRACT: Frank–Shockley partial dislocations, with lines parallel to the ⟨10$\bar{1}$0⟩ direction, were studied in wurtzite GaN using atomistic calculations, based on density functional theory, and high resolution scanning transmission electron microscopy. Two types of dislocations were considered, that is, mixed 55° and 73°, with core configurations in their vacancy and interstitial variants of both gallium or nitrogen polarity. The core configurations of the mixed 55° dislocation have a structure with a 7-atom ring, involving both gallium and nitrogen dangling bonds, associated with shallow gap states. The core configurations of the mixed 73° dislocation with gallium polarity have a 3/5-atom ring structure, whereas those with nitrogen polarity have a structure with a 6-atom ring. These core configurations were found to be associated with both shallow and deep gap states, where the latter are due to either Ga–Ga bonds or interacting nitrogen dangling bonds. It was demonstrated that a direct discrimination between vacancy and interstitial core variants of the same partial dislocation, in a high resolution transmission electron microscopy observation, is impossible along the *m*-direction, unless the sample is rotated by ± 30° around the ⟨0001⟩ axis. This rotation reveals the I1 basal stacking fault, enabling its location to be determined in relation to the extra half-plane associated with the **c**/2 component. It also allows the core variant of the partial dislocation to be determined. Knowledge of the core structures of the *m*-line Frank–Shockley partial dislocation allowed for the decryption of the dissociation of the a + c edge dislocation, observed by high-resolution scanning transmission electron microscopy, which is involved in the relaxation of strain at the technologically relevant InGaN/GaN interfaces.

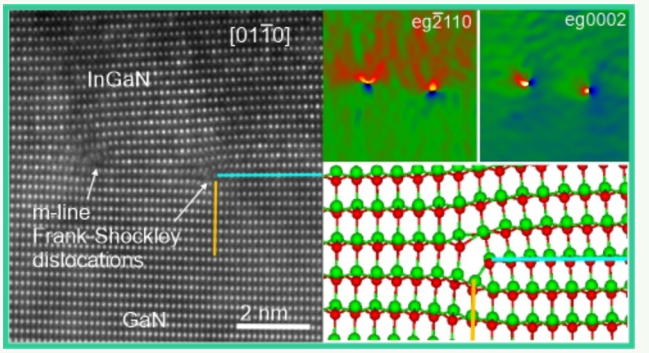

KEYWORDS: *GaN, DFT, HRSTEM, Frank–Shockley, partial dislocations, dislocation cores, electronic properties*

1. INTRODUCTION

Over the last two decades, III-nitride semiconductors have become relevant in many modern technologies.[1] These materials, with a hexagonal wurtzite structure, constitute an alloy system with direct bandgaps covering a wide range of the electromagnetic spectrum, from the ultraviolet to the infrared regions,[2] and are employed, among others, in the fabrication of light emitters such as LEDs and laser diodes that exhibit high internal quantum efficiency and high brightness. Thus, III-nitride semiconductors have been at the heart of a revolution in the solid-state lighting industry.[1]

The growth of III-nitride semiconductors is usually achieved using heteroepitaxial techniques on mismatched foreign substrates.[3] Consequently, the resulting epilayers exhibit structural defects such as dislocations and planar defects.[4,5] Basal stacking faults (BSFs) are frequent planar defects, that arise from the disturbance of the normal stacking sequence of atomic planes along the [0001] direction.[6] Among BSFs, the I1 type is the most frequent one, as it has the lowest formation energy.[7,8] III-nitride epilayers contain different types of dislocations, such as threading, misfit and partial dislocations (PDs).[9] Threading dislocations are the most abundant type of dislocations in III-nitride materials.[10] These lattice dislocations penetrate the entire epilayer, adversely impacting the performance and lifetime of electronic devices.[11,12] Misfit dislocations are localized at the heteroepitaxial interfaces[13] and are introduced to accommodate the lattice mismatch and relax

Received: April 28, 2025
Revised: June 18, 2025
Accepted: June 19, 2025

the interfacial strain[14] when the epilayer thickness exceeds a critical value.[15] PDs delimit stacking faults.[16] They are created either through the introduction of stacking faults during epitaxial growth or by the dissociation of perfect dislocations. In the wurtzite structure, Shockley PDs bounding I2 type BSFs, and Frank−Shockley (F−S) PDs, bounding I1 BSFs, can have either *a*-type line directions, i.e., parallel to $\langle 11\bar{2}0\rangle$, or *m*-type, i.e., parallel to $\langle 10\bar{1}0\rangle$.[17,18] *A*-line PDs have been investigated more extensively than *m*-line ones.[19,20] The atomic and electronic structures of the core configurations of *a*-line F−S PDs were determined in wurtzite GaN.[21,22] The core structures determined by atomistic calculations were confirmed by high-resolution transmission electron microscopy (HRTEM).[16] Despite their relevance, no reports have been published thus far on the cores and electronic structures of *m*-line PDs in III-nitrides. Currently, only perfect *m*-line dislocations have been investigated in GaN.[23,24]

F−S *m*-line PDs have been associated with important processes in III-nitride semiconductors such as the nucleation of **a**-type threading dislocations,[25] as well as the interfacial relaxation between III-nitride epilayers.[14] Smalc−Koziorowska et al.[8] observed that reactions between m-line F−S PDs surrounding hexagonal BSF domains can be sources of a-type threading dislocations in III-nitride heterostructures. Furthermore, it was demonstrated that the strain relaxation of InGaN epilayers grown along the [0001] direction on GaN templates proceeds via the introduction of **a** + **c** misfit dislocations.[26] These edge dislocations glide on the $(11\bar{2}2)$ pyramidal plane and dissociate into *m*-line F−S PDs, which allows for an effective release of the interfacial strain.[14,26] Therefore, investigating *m*-line F−S PDs and determining their core properties are essential to address central issues in III-nitride semiconductors.

The present work is dedicated to the investigation of the properties of F−S PDs with *m*-lines in wurtzite GaN. Their electronic structures, core configurations, and relative stability were determined. For that purpose, atomistic calculations based on density functional theory (DFT) were performed. The obtained results were employed to describe the dissociation of the **a** + **c** misfit dislocation which is responsible for the relaxation of strain at the InGaN/GaN. The manuscript is organized as follows: In Section 2, the structure of BSFs in the wurtzite structure as well as the geometrical features of F−S PDs with *m*-lines are recalled. In Section 3, the computational settings adopted in the calculations are described. Section 4 is dedicated to the presentation of the obtained results concerning the core configurations of F−S PDs, their energetics, and electronic structures. In section 5, the obtained results are summarized and conclusions are drawn.

2. I_1 BASAL STACKING FAULT AND THE *M*-LINE FRANK−SHOCKLEY PARTIAL DISLOCATION

BSFs are the most frequently observed planar defects in III-nitride materials.[27] They comprise an alteration of the stacking sequence of the (0002) basal planes, resulting in the introduction of zinc blende structural units in the wurtzite structure. Different types of BSFs have been reported, denoted as I_1, I_2, I_3, and E.[7] The BSF types differ mainly in the number of introduced zinc blende structural units and are formally characterized by their displacement vectors.[7] The I_1 BSF has the lowest formation energy, and the E BSF the highest one.[7,8] Recently, we reported a new BSF type, which we named I_4, that plays a key role in explaining the origin of threading dislocations in III-nitride epilayers.[8,25]

Figure 1 shows the stacking of (0002) basal planes in a perfect wurtzite structure and in an I_1 BSF. In the wurtzite

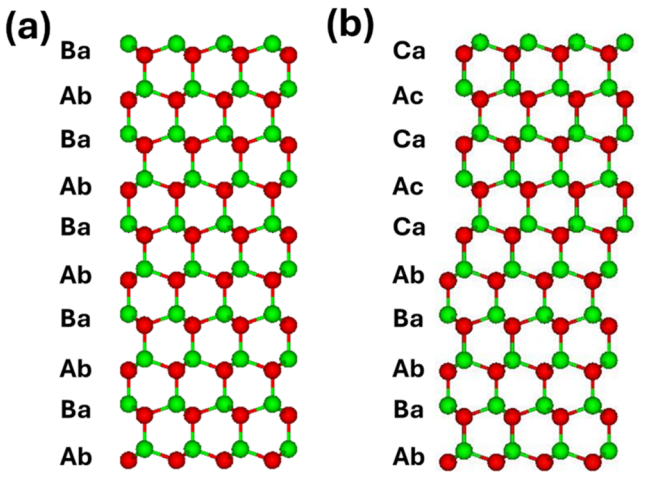

Figure 1. Stacking of (0001) basal planes in wurtzite GaN, projected along the $[11\bar{2}0]$ direction. (a) Perfect wurtzite structure. (b) I_1 BSF. (Green balls represent gallium atoms and red ones nitrogen atoms.).

structure, the stacking of the atomic planes along the $\langle 0001\rangle$ direction can be described by the sequence... *AaBbAaBbAaBbAaBbAaBb*..., where capital letters refer to N atoms and lowercase to Ga atoms. By introducing an I_1 BSF, the stacking sequence of the wurtzite structure is locally violated and becomes... *AaBbAaBbAaBbAaCcAaCcAa*... The modification of the stacking sequence in an I_1 BSF leads to the introduction of a single row of zinc blende structural units. Crystallographically, an I_1 BSF can be created by either removing or adding an (0002) basal bilayer (e.g., *Ba*) and then applying a $1/3\ \langle 10\bar{1}0\rangle$ shear. The application of the previous two-step process leads to a total displacement vector of $\boldsymbol{p} = 1/6\ \langle 02\bar{2}3\rangle$.

The I_1 BSF is delimited by a F−S PD loop with Burgers vector $\boldsymbol{b} = 1/6\ \langle 02\bar{2}3\rangle$. In the wurtzite structure a F−S PD with a line direction parallel to the *m*-direction, can be of two types: either mixed 55° or mixed 73°. The Burgers vectors of the mixed dislocations have two components: an edge ($\boldsymbol{b}_e$) and a screw component ($\boldsymbol{b}_s$), such that $\boldsymbol{b} = \boldsymbol{b}_e + \boldsymbol{b}_s$. The edge component is associated with the introduction of extra half-planes. The mixed 55° dislocation has a $1/2\ \langle 0001\rangle$ edge component which introduces a (0001) extra half-plane, hereafter called the **c**/2 component. Then, the Burgers vector of the mixed 55° dislocations can be written as $\boldsymbol{b}_{55} = \boldsymbol{b}_e + \boldsymbol{b}_s = 1/2\ \langle 0001\rangle + 1/3\ \langle 10\bar{1}0\rangle$ (Figure 2a). The mixed 73° has two edge components. The $1/2\ \langle 0001\rangle$ component and the $1/6\ \langle 1\bar{2}10\rangle$ edge component, which that introduces an additional $(1\bar{2}10)$ half-plane (hereafter called the **a**/2 component). The Burgers vector of the mixed 73° dislocation can then be written as $\boldsymbol{b}_{73} = (\boldsymbol{b}_{e1} + \boldsymbol{b}_{e2}) + \boldsymbol{b}_s = 1/2\ \langle 0001\rangle + 1/6\ \langle 1\bar{2}10\rangle + 1/6\ \langle 10\bar{1}0\rangle$ (Figures 2b,c). Thus, one main difference between the two F−S PDs is that the mixed 55° has only one additional extra half-plane while the mixed 73° dislocation has two which are perpendicular to each other. Two physical mechanisms are associated with the formation of the I_1 BSF domains, i.e., condensation of an interstitial or collapse of a vacancy disk (Figure 3a,b).[21] These are consistent with the crystallographic process of creating I_1 BSFs by adding or removing atoms, as

https://doi.org/10.1021/acsaelm.5c00859
ACS Appl. Electron. Mater. XXXX, XXX, XXX−XXX

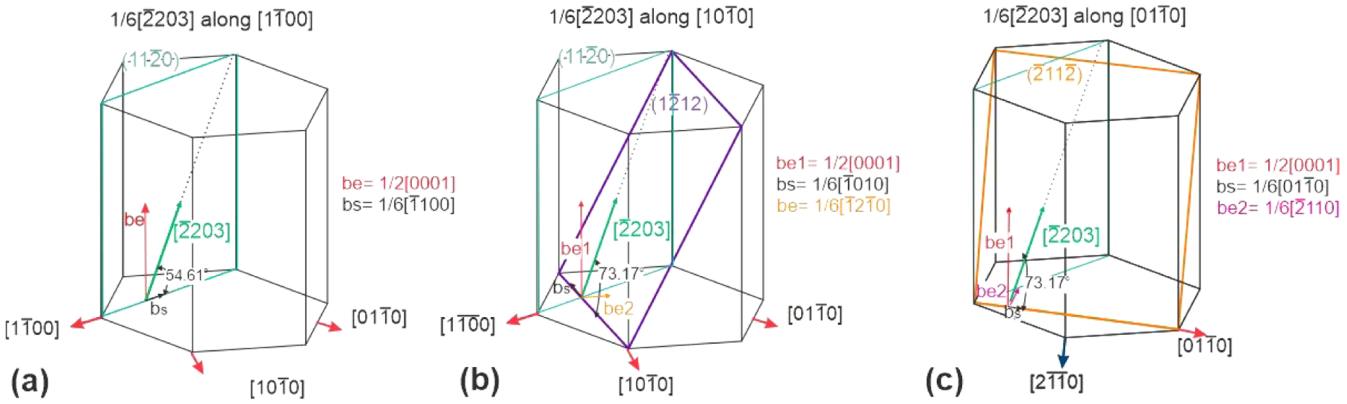

Figure 2. Schematic representation of the line directions and the Burgers vectors of the mixed 55° F−S PD (a) and the mixed 73° F−S PD (b), (c).

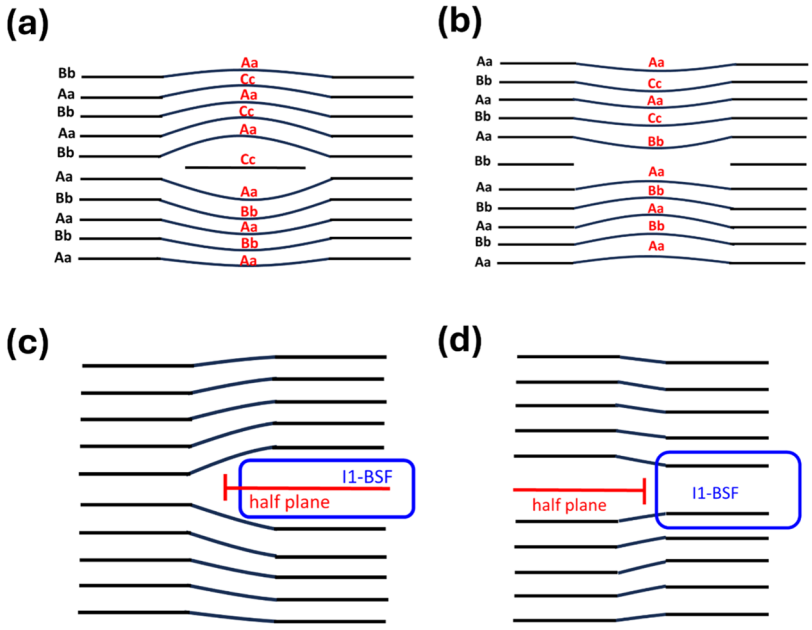

Figure 3. Schematic representation of the stacking sequence associated with an I_1 BSF, in the case of (a) condensation of an interstitial disk or (b) collapse of a vacancy disk. A representation of the mutual positions of the extra half-plane and the I_1 BSF in (c): the F−S PD at the border of the interstitial disk and (d): the F−S PD at the border of the vacancy disk.

described previously. Depending on the mechanism of creation of the I_1 BSF, a F−S PD admits two structural variants, i.e., the interstitial and vacancy variant.

3. COMPUTATIONAL AND EXPERIMENTAL METHODS

F−S PDs with $\langle 10\bar{1}0\rangle$ *m*-lines were modeled in wurtzite GaN by using supercell-cluster hybrids.[28,29] The latter have nearly rectangular parallelepiped shapes with sides along the $\langle 0001\rangle$, $\langle 11\bar{2}0\rangle$ and $\langle 10\bar{1}0\rangle$ directions, and sizes ranging between 380 and 400 atoms. The supercell-cluster hybrids were naturally periodic along the dislocation line direction with a periodicity of $a\sqrt{3}$, where a is the basal lattice parameter. They were finite along the transversal directions while expanding over approximately 28 Å on the $(10\bar{1}0)$ plane. The lateral surfaces of the models were saturated with pseudohydrogen atoms to emulate bulk GaN. Thus, dangling bonds at gallium and nitrogen atoms were capped by fractionally charged 1.25e and 0.75e hydrogen atoms, respectively.[28,29] Periodic boundary conditions were applied on the $(10\bar{1}0)$ plane while including a vacuum as large as 25 Å. This prevents interactions between the physical model and those generated by the application of periodic boundary conditions.

Initial atomic positions of the *m*-line F−S PD were generated by application of the displacement field from isotropic elasticity theory.[30] Equilibrium atomic positions were obtained through atomic relaxation, achieved by using the conjugate gradients algorithm.[31] The adopted convergence criterion was that the difference in energy between two subsequent atomic configurations is below 10^{-5}Ha. All the atoms were allowed to relax, but those at the lateral surfaces of the model were kept fixed. The evaluation of energies and forces was achieved in the framework of density functional theory (DFT).[32,33] The calculations were carried out by using the AIMPRO (Ab-Initio Modeling PROgram) code[34] which is based on pseudopotentials and an expansion of the valence electron wave functions on a basis set of Cartesian Gaussian orbitals.[34] Norm-conserving Hartwingsen-Geodecker-Hutter pseudopotentials[35] were employed to describe nuclei and core electrons. The considered valence was composed of Ga-3d, Ga-4s, Ga-4p, N-2s, N-2p and H-1s electrons. The valence electronic wave functions were expanded into an uncontracted {*dddd*} basis set of 40 atom-centered (Ga or N) Gaussian functions and a contracted C44G* basis set of 13 atom-centered (H) Gaussian functions. The charge density was developed in an auxiliary basis set of plane waves with a size corresponding to 500 Ry. The exchange and correlations were treated in the framework of the Local Density Approximation

https://doi.org/10.1021/acsaelm.5c00859
ACS Appl. Electron. Mater. XXXX, XXX, XXX−XXX

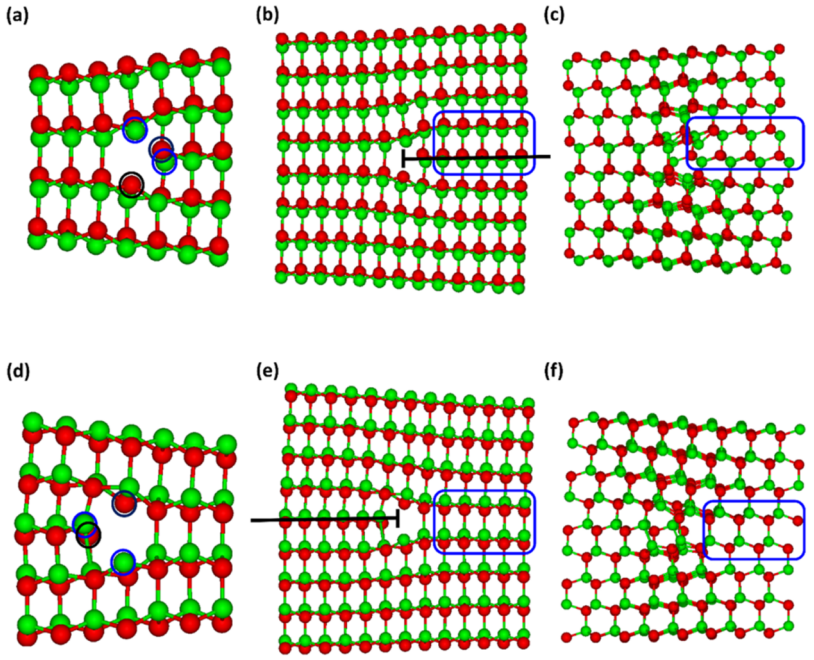

Figure 4. Ball-and-stick models of the core configurations of the 55° F−S PD in GaN. Atoms are as in Figure 1. (a), (d): Atomic structures of the 55°-Int and 55°-Vac core configurations, respectively. Black and blue circles represent atoms having N- and Ga-dangling bonds, respectively. (b), (e): Representations of the extra half-planes and the I_1 BSF in the 55°-Int and 55°-Vac core configurations, respectively. The **c**/2 component is indicated in black, and the I_1 BSF is delimited in blue. (c), (f): 30° rotated models around the *c*-axis, showing the I_1 BSF delimited in blue.

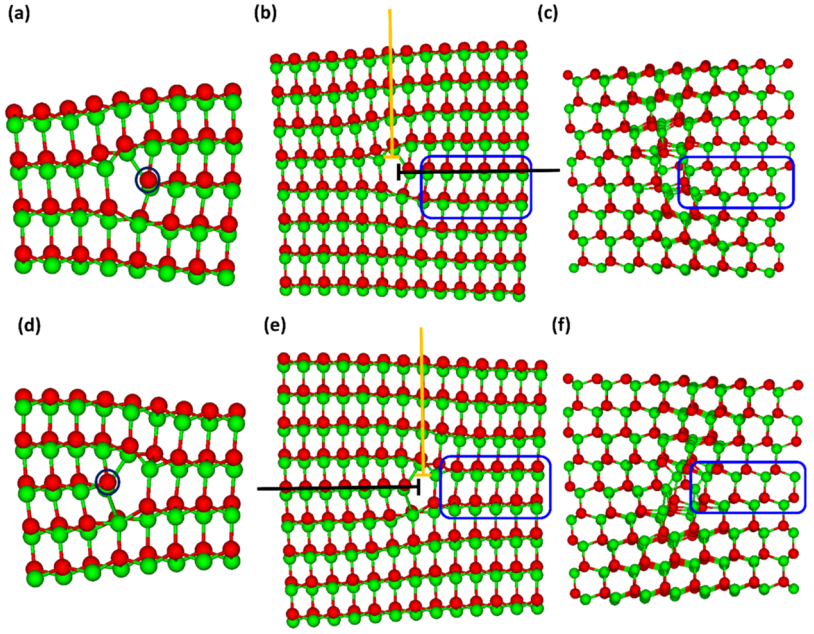

Figure 5. Ball and stick models of the core configurations of the 73° F−S PD with Ga polarity in GaN. Atoms are as in Figure 1. (a), (d): Atomic structures of the 73°-Int-Ga and 73°-Vac-Ga core configurations, respectively. Black circles represent atoms having N-dangling bonds. (b), (e): Representations of the extra half-planes and the I_1−BSF in the 73°-Int-Ga and 73°-Vac-Ga core configurations, respectively. The **c**/2 component is in black, the **a**/2 component in yellow, and the I_1−BSF is delimited in blue. (c), (f): 30° rotated models around the *c*-axis, showing the I_1−BSF delimited in blue.

(LDA), where the Perdew−Wang (PW92) functional was used.[36] Integrations over the Brillouin Zone were evaluated within the Monkhorst−Pack scheme.[37] A (0.5, 0.5, 0.5) shifted [1 × 1 × 8] homogeneous grid with four symmetry-reduced *k*-points along the *m*-direction, was used. The electron occupation of the Kohn−Sham energy levels was performed according to the first-order Methfessel−Paxton function[38] while using a smearing energy of 0.01 eV.

The performance of our adopted computational scheme was tested by reproducing some of the physical properties of bulk wurtzite GaN. The calculated lattice parameters a = 3.161 Å and c = 5.153 Å were in excellent agreement with the experimental values of a = 3.190 Å and c = 5.189 Å.[39] Otherwise, the calculated elastic constants were (in GPa): C_{11} = 370.6, C_{12} = 152.7, C_{13} = 103.4, C_{33} = 419.9, C_{44} = 8 3.0 and C_{66} = 108.9. These values were in good agreement with the experimentally measured elastic constants: C_{11} = 390, C_{12} = 145, C_{13} =

https://doi.org/10.1021/acsaelm.5c00859
ACS Appl. Electron. Mater. XXXX, XXX, XXX−XXX

106, C_{33} = 398, C_{44} = 105, and C_{66} = 125,[40] within the limits of the error bars admitted in DFT.

The *m*-line F−S PDs were observed experimentally at the $In_{0.2}Ga_{0.8}N/GaN$ interface in epitaxial structures deposited by molecular beam epitaxy (MBE). The studied structures were grown on bulk GaN substrates obtained via ammonothermal growth (threading dislocation density of ∼ 10^4 cm^{-2}). The miscut of the substrates was in the range of 0.3−0.5° toward the $[1\bar{1}00]$ direction. We carried out structural studies employing transmission electron microscopy (TEM) and scanning-transmission electron microscopy (STEM) using an FEI Tecnai G2 F20 S-TWIN and a Thermo Fischer Scientific Spectra200, both operated at 200 kV and equipped with high-angle annular dark field (HAADF) STEM detectors. The bright field STEM (BF-STEM) detector was used for studying the polarity of studied layers. Observations were performed in cross-section along the $\langle 11\bar{2}0\rangle$ and $\langle 10\bar{1}0\rangle$ zone axes. Specimen preparation was performed by mechanical polishing, followed by ion milling in the PIPS system (Gatan). Geometrical phase analysis (GPA) was applied to high resolution STEM (HRSTEM) images in order to show the in-plane and out-of-plane strain components of the partial dislocations.

4. RESULTS AND DISCUSSION

4.1. Atomic Structure and Core Configurations. The mixed 55° and 73° F−S PDs with *m*-lines were considered in their two variants, i.e., vacancy and interstitial. As indicated previously, the latter discrimination is based on the physical mechanisms associated with the creation of the dislocation. Here, we introduce an alternative easy way of distinguishing between the vacancy and interstitial variant, which is based on the position of the extra half-plane of the **c**/2 component relevant to the I_1 BSF. In the interstitial variant, both the extra half-plane and the I_1 BSF are located on the same side of the core (Figure 3c), whereas, in the vacancy variant, they are situated on opposite sides (Figure 3d).

Different core configurations were investigated for the F−S PDs in their vacancy and interstitial variants. These configurations were generated by placing the origin of the elastic displacement field of the dislocation at different positions between the (0001) or $(11\bar{2}0)$ planes.[41] By adopting this strategy, six stable core configurations were identified, two for the 55° and four for the 73° PD. The two core configurations of the 55° PD are denoted as 55°-Int for the interstitial variant and 55°-Vac for the vacancy variant (Figure 4). The presence of the **a**/2 Burgers vector component leads to a multiplication of the core configurations of the mixed 73° PD.

Indeed, the extra half-plane associated with the **a**/2 component terminates at the dislocation core with a single row of low-coordinated atoms that can be formed by either Ga or N atoms. This induced core polarity (Ga or N) doubles the number of configurations for both the interstitial and vacancy variants, leading to four core configurations denoted as 73°-Int-Ga, 73°-Int-N, 73°-Vac-Ga, and 73°-Vac-N (Figures 4 and 5).

The core configuration of an F−S PD is described in terms of rings formed by the closest atomic columns to the core's center when the dislocation is viewed along its line direction. Such a description is convenient and easy to implement in wurtzite GaN, especially in the case of dislocations with lines parallel to the [0001] *c*-direction[41] or to the <11$\bar{2}$0> *a*-direction,[20] where individual atomic columns are well resolved by HR(S)TEM. In the case of the *m*-direction, the Ga and N atomic columns are arranged close to each other, effectively giving rise to Ga/N 'bicolumns'. Thus, as described in our previous report,[18] the core structure of an *m*-line dislocation is best described in terms of rings formed by Ga/N bicolumns instead of individual atomic columns.

Figure 4 illustrates the core configurations of the mixed 55° F−S PD. Figure 4b presents the 55°-Int configuration and clearly shows that the dislocation comprises a single extra half-plane, owing to the **c**/2 edge component. When the dislocation is viewed edge-on along the $\langle 10\bar{1}0\rangle$ direction, the I_1 BSF is not discernible. To make it visible, the model has to be rotated around the ⟨0001⟩ axis by ± 30°, as shown in Figure 4c. As the extra half-plane and I_1 BSF are both located on the same side of the core, this confirms the interstitial character of the partial dislocation. Figure 4e,f represent the 55°-Vac configuration, showing the extra half-plane and the I_1 BSF on opposite sides of the core, which confirms the vacancy character of the dislocation. Figure 4a,d show the core configurations of the mixed 55 °Frank-Shockley partial dislocation, i.e., 55°-Int and 55°-Vac, to have an atomic structure with a 7-atom ring, involving both Ga- and N-dangling bonds. The detailed atomic structures of the core configurations of the 55° F−S PD, in terms of bond deformations and bond angles, are summarized in Table 1. The criterion used to assess the formation of a Ga−N bond is mainly geometrical. Any Ga−N bond stretched by more than 20% relative to its equilibrium length, i.e., 1.95 Å, is considered broken. Moreover, the local environment of atoms with overstretched bonds was analyzed. Indeed, when a bond is broken, the resulting dangling bond typically induces a relaxation (i.e., a contraction) of the surrounding bonds. In the 55°-Int configuration, the most stretched bonds are deformed at +7.7%, and the most compressed ones are at −6.4%, while the bond angle dispersion ranges from 88.3° to 126.7°. In the 55°-Vac configuration, the most stretched bonds are deformed by +8.6%, and the most compressed ones are at −7.11%, while the bond angles vary from 93.7° to 127.4°.

Table 1. Bond Deformations and Bond Angles at Different Core Configurations of the 55° and 73° Frank−Shockley Partial Dislocations

dislocation	core configuration	bond deformations (%) (compression/extension)	bond angles (°) (min−max)
55°	Int	−6.4%/+7.7%	88.3°−126.7°
	Vac	−7.1%/+8.6%	93.7°−127.4°
73°	Int-Ga	−5.5%/+14.9%	90.8°−132.1°
	Int-N	−7.4% /+16.4%	94.0°−129.3°
	Vac-Ga	−5.2% /+11.7%	92.2°−131.8°
	Vac-N	−7.2% /+19.8%	96.0°−128.9°

Figures 5 and 6 illustrate the mixed 73° F−S PD in its interstitial and vacancy variants with Ga and N polarities. Figures 5b,e and 6b,e show the dislocation to have two perpendicular extra half-planes, associated with the **c**/2 and **a**/2 edge components. Figures 5c,f and 6c,f illustrate rotated models around the ⟨0001⟩ axis by ± 30°, which makes visible the I_1 BSF along the $\langle 11\bar{2}0\rangle$ direction. Figures 5a−c and 6a−c represent interstitial configurations of the 73° dislocation as the extra half-plane, associated with the **c**/2 component, and the I_1 BSF are located on the same side of the core. The vacancy configurations are shown in Figures 5d−f and 6d−f, whereby the extra half-plane associated with the **c**/2 component, and the I_1 BSF are located on opposite sides of the core. The inspection of the nature of the atoms at the bottom of the extra half-planes associated with the **a**/2 edge component indicates that Figure 5 comprises cores with Ga

https://doi.org/10.1021/acsaelm.5c00859
ACS Appl. Electron. Mater. XXXX, XXX, XXX−XXX

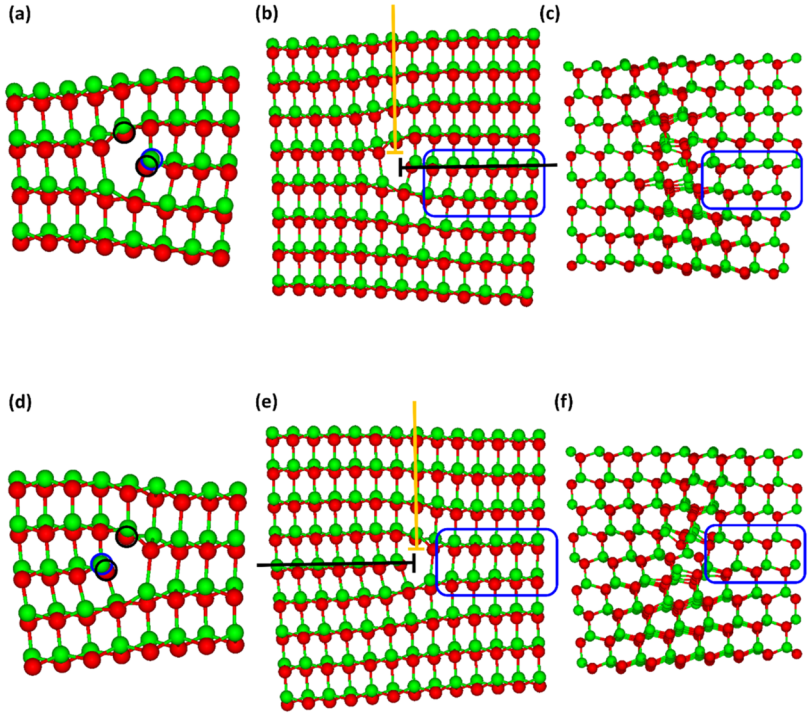

Figure 6. Ball and stick models of the core configurations of the 73° F−S PD with N polarity in GaN. Atoms are as in Figure 1. (a), (d): Atomic structures of the 73°-Int-N and 73°-Vac-N core configurations, respectively. Black and blue circles represent atoms having N- and Ga-dangling bonds, respectively. (b), (e): Representations of the extra half-planes and the I_1−BSF in the 73°-Int-N and 73°-Vac-N core configurations, respectively. The **c**/2 component is in black, the **a**/2 component in yellow and the I_1−BSF is delimited in blue. (c), (f): 30° rotated models around the *c*-axis, showing the I_1−BSF delimited in blue.

polarity, whereas Figure 6 illustrates those with N polarity. The detailed atomic structures of the core configurations of the 73° F−S PD are summarized in Table 1.

The cores of the 73° F−S PD with Ga polarity (Figure 5) exhibit a configuration with a 3:5-atom ring structure, involving Ga−Ga bonds and N-dangling bonds. The 73°-Int-Ga core configuration involves Ga−Ga homonuclear bonds with a length of 2.49 Å, while those in the 73°-Vac-Ga have a length of 2.44 Å. In the 73°-Int-Ga core configuration, the most extended Ga−N bonds are deformed by +14.9%, and the most compressed ones are at −5.5%. The bond angles ranged from 90.8° to 132.1°. The 73° F−S PD, in both vacancy and interstitial variants, with N polarity (Figure 6) exhibits a core configuration with a 6-atom ring structure, involving both N- and Ga-dangling bonds. The 73°-Int-N configuration involves Ga−N bonds, where the most compressed ones are deformed at −7.4% and the most extended ones are at +16.4%. It exhibits a bond angle dispersion from 94.0° to 129.3°. In the 73°-Vac-N core configuration, Ga−N bonds are established, where the most compressed bonds are at −7.2% and the most extended ones are at +19.8%. The bond angles vary between 96.0° and 128.9°.

4.2. Energetics. The formation energy of a dislocation is defined as the difference between the energies of the defected system (E_{dis}) and the perfect bulk crystal (E_{perf})

$$E_f = E_{dis} - E_{perf} \tag{1}$$

where the two systems must have the same number of atoms. The formation energy of a partial dislocation has three contributions and can be expressed as follows

$$E_f = E_{el} + E_c + E_{sf} \tag{2}$$

E_{el} is the elastic energy, E_c the core energy, and E_{sf} the energy of the stacking fault delimited by the dislocation. The elastic contribution can be accurately determined within linear elasticity theory,[42] whereas the core energy requires atomistic calculations for its evaluation. The stacking fault energy has a constant value per unit area. The elastic energy, which constitutes the largest contribution to the formation energy of a dislocation, can be expressed as[42]

$$E_{el}(r) = \left(\frac{1}{4\pi}\right) b^2 K(\alpha) \ln\left(\frac{r}{r_c}\right) \tag{3}$$

It represents the elastic energy per unit length stored in a cylinder of radius r around the dislocation, with b being the magnitude of the Burgers vector and r_c the core radius. $K(\alpha)$ represents the energy factor and can be expressed in the framework of isotropic elasticity theory as[42]

$$K(\alpha) = G\left(\cos^2\ \alpha + \frac{\sin^2\ \alpha}{1 - \nu}\right) \tag{4}$$

where G and v represent, respectively, the shear modulus and the Poisson ratio of the material, and α is the angle between the Burgers vector and the dislocation line.

The relative stability of the two F−S PDs, that is, the mixed 55° and the mixed 73°, can be determined by inspecting their elastic energy, which constitutes the largest contribution to their formation energies. This can be directly reflected through the values of their energy factors: $K(55°)$ = 0.813 eV/Å and $K(73°)$ = 0.986 eV/Å, which indicate that the 55° partial dislocation is easier to create than the 73° one.

The energetic hierarchy of different core configurations of the two F−S PDs, the mixed 55° and 73°, was established by

https://doi.org/10.1021/acsaelm.5c00859
ACS Appl. Electron. Mater. XXXX, XXX, XXX−XXX

evaluating their relative formation energies (ΔE_f). For two configurations of the same F−S PD, the relative formation energy is the difference in their core energies, as the respective stacking fault and elastic contributions cancel out. The relative formation energies of the core configurations of the mixed 55° and 73° were evaluated using iso-stoichiometric models, and the obtained values are summarized in Table 2.

Table 2. Relative Formation Energies of Different Core Configurations of the 55° and 73° Frank−Shockley Partial Dislocations[a]

dislocation	core configuration	ΔE_f (meV/Å)
55°	Int	x
	Vac	65.51
73°	Vac-Ga	x
	Int-Ga	197.06
	Vac-N	251.21
	Int-N	283.80

[a]The interstitial and vacancy core configurations with gallium polarity were adopted as reference for the evaluation of the relative formation energies of the 55° and 73° dislocations, respectively.

For the 55° dislocation, the interstitial variant of the core was found to be more energetically favorable than the vacancy one (Table 2). However, the vacancy variants of the core configurations of the 73° dislocation, with either gallium or nitrogen polarity, were found to be the most energetically favorable (Table 2). Overall, for the core configurations of the 73° dislocation, Vac-Ga was identified as the ground-state configuration, whereas Int-N exhibited the highest formation energy. The vacancy and interstitial variants of the core with nitrogen polarity are closer in energy (32.6 meV/Å) than those with gallium polarity (197.1 meV/Å).

4.3. Electronic Structure. The electronic structures of the core configurations of both 55° and 73° F−S PDs were determined by performing Density Of States (DOS) calculations. The atomic origin of the dislocation-associated gap states was identified by the graphical representation of the squared module of the electronic wave function.[20,41]

Figure 7 shows the electronic structures of the two core configurations of the 55° F−S PD. Both core configurations, vacancy and interstitial variants, share the same electronic structure, which is characterized by the presence of solely shallow gap states. The occupied gap states situated just above the Valence Band Maximum (VBM) are due to N-dangling bonds (Figure 7a). However, the unoccupied gap states situated just below the Conduction Band Minimum (CBM) are due to localized interacting Ga-dangling bonds (Figure 7b).

Figure 8 shows the electronic structures of the four core configurations of the 73° F−S PD. In contrast to the 55° dislocations, these dislocations possess electronic structures including both shallow and deep gap states. The core configurations, vacancy and interstitial variants, with the same polarity, Ga or N, were found to have identical electronic structures. In the core configurations with Ga polarity (Figure 8a,b), the deep gap states are induced by the Ga−Ga bonds formed in the core, while the occupied shallow gap states, located just above the VBM are localized on the N-dangling bonds. However, in the core configurations with N polarity (Figure 8c,d), the deep gap states are due to interacting N-dangling bonds, whereas the unoccupied shallow gap states, located just below the CBM, are introduced by interacting Ga-dangling bonds.

4.4. Dissociation of the Edge a + c Lattice Dislocation. F−S PDs can result from the dissociation of perfect dislocations. This process allows perfect dislocations to decrease their energies.[42] In a hexagonal crystal, an **a** + **c** dislocation can dissociate into two F−S PDs, separated by an I_1−BSF ribbon, according to the following reaction

$$1/3[2\bar{1}\bar{1}3] \rightarrow 1/6[20\bar{2}3] + 1/6[2\bar{2}03] + I_1 \text{ BSF} \quad (5)$$

In wurtzite III-nitride semiconductors, the presence and dissociation of **a** + **c** dislocations play an important role in the relaxation of the interfacial strain between epilayers grown along the [0001] direction.[43,44] Hereafter, HRSTEM images of a dissociated **a** + **c** dislocation are analyzed, in light of the structural results obtained in Section 4.1, to identify the type and structure of the core configurations of the involved F−S PDs.

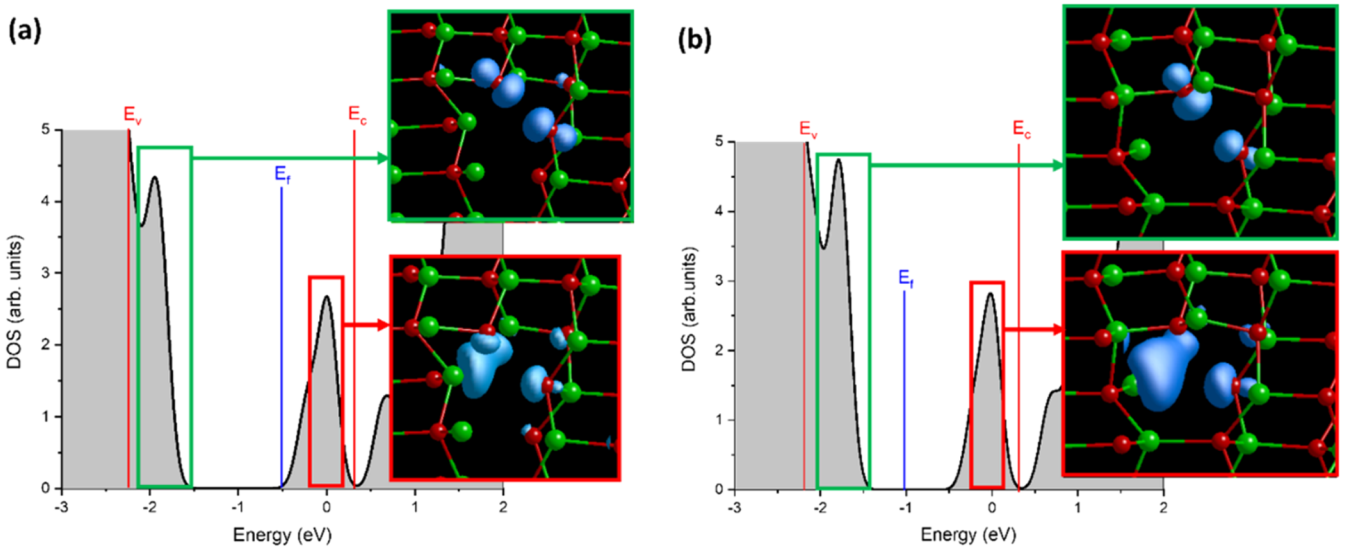

Figure 7. Electronic structures of the core configurations of the 55° F−S PD in GaN. Atoms are as in Figure 1. Insets represent the squared module of the electronic wave function associated with different gap states. (a) The 55°-Int core configuration. (b) The 55°-Vac core configuration.

https://doi.org/10.1021/acsaelm.5c00859
ACS Appl. Electron. Mater. XXXX, XXX, XXX−XXX

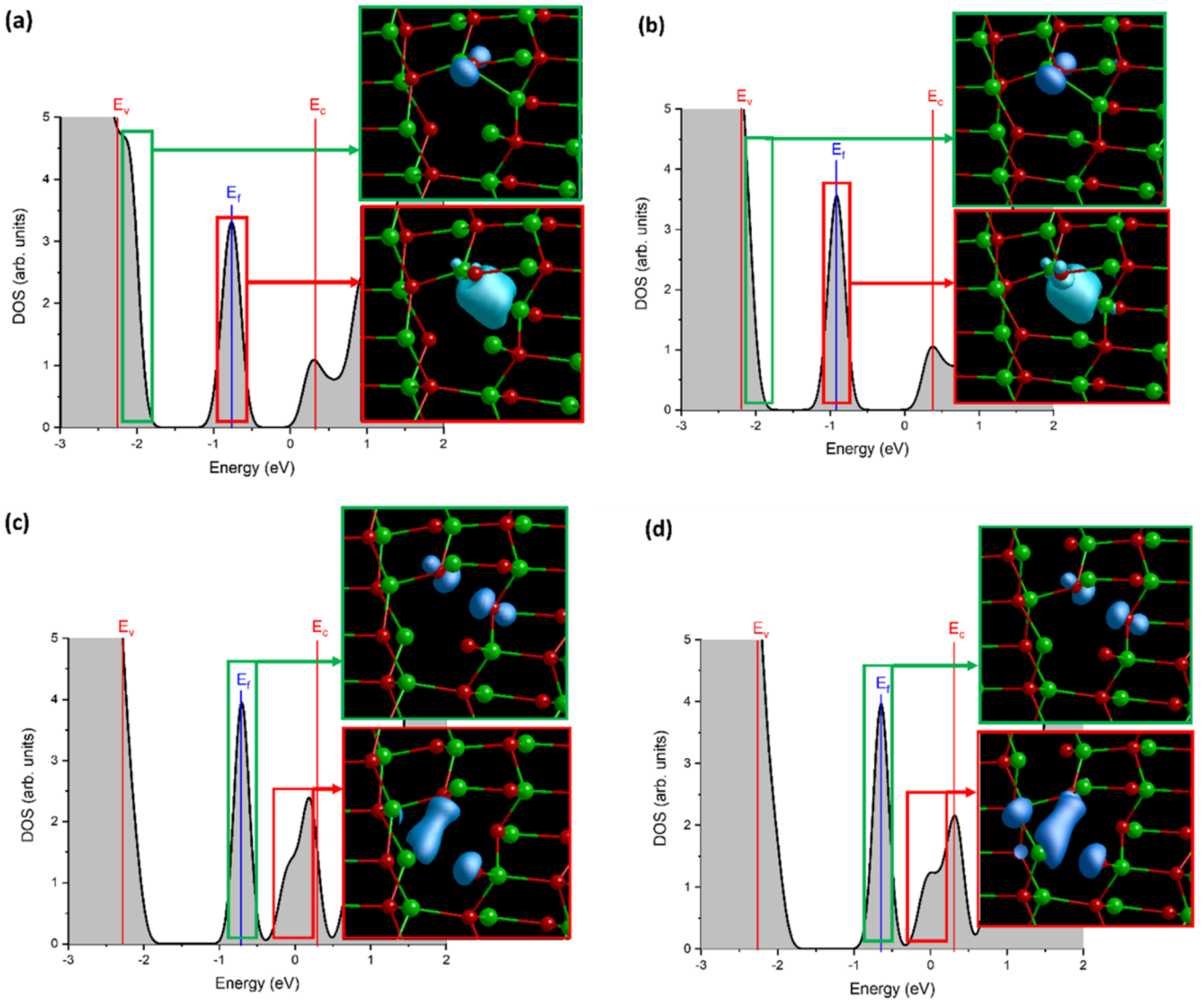

Figure 8. Electronic structures of the core configurations of the 73° F−S PD in GaN. Insets represent the squared module of the electronic wave function associated with different gap states. (a) The 73°-Int-Ga core configuration. (b) The 73°-Vac-Ga core configuration. (c) The 73°-Int-N core configuration. (d) The 73°-Vac-N core configuration.

Figures 9a and 10a illustrate cross sectional HRSTEM images of a dissociated edge **a** + **c** dislocation, with an *m*-line, into two F−S PDs at the InGaN/GaN interface. In Figure 9a, the dislocations are recorded edge-on along the $[01\bar{1}0]$ zone axis, whereas, in Figure 10a, the sample is rotated by 30° to the $[11\bar{2}0]$ zone axis in order to make the I_1 BSF visible. The respective projections of the atomistic model of the dissociated edge dislocation in wurtzite GaN are shown in Figures 9f and 10f. In the projection direction of Figure 9a, the I_1 BSF separating the two F−S PDs, hereafter called left and right one, is not structurally discernible.

On the contrary, the I_1 BSF is well visible in Figure 10a. The width of the BSF ribbon is approximately 35.5 Å. A Burgers circuit applied around the whole configuration in Figure 9a, i.e., surrounding the two partials, leads to a closure failure of 1:3 $\langle 2\bar{1}\bar{1}3\rangle$ which corresponds to the Burgers vector of an edge **a** + **c** dislocation. The two F−S PDs are of the same type and exhibit two perpendicular extra half-planes (Figure 9a). This dismisses the mixed 55° as a candidate, as it has only one extra half-plane, and suggests that the two partials are mixed 73°. The Burgers circuit performed around each F−S PD leads to a closure failure with a vector 1/6 $\langle 1\bar{2}13\rangle$ that corresponds to the Burgers vector of the edge component of the 73 °Frank-Shockley partial dislocation. The double extra half-planes of each PD are also well discernible in the lattice strain maps obtained by GPA and in the Bragg filtered images (Figure 9b−e). We note that, in Figure 10a., only one of the two PDs appears to comprise two extra half-planes but this is misleading since the dislocation lines are not edge-on. The inspection of the relative position of the extra half-plane associated with the **c**/2 component and the I_1 BSF (Figure 9a) indicates that the left partial dislocation has an interstitial core structure variant, whereas the right dislocation has a vacancy core structure variant. Indeed, in the left dislocation, the extra half-plane associated with the **c**/2 component and the I_1 BSF are located on the same side of the core, whereas in the right dislocation, they are located on opposite sides of the core (Figures 9a and 10a). As demonstrated in Section 4.1, two different core structures are possible depending on the polarity of the core, i.e., the nature of the atomic column at the bottom of the extra

https://doi.org/10.1021/acsaelm.5c00859
ACS Appl. Electron. Mater. XXXX, XXX, XXX−XXX

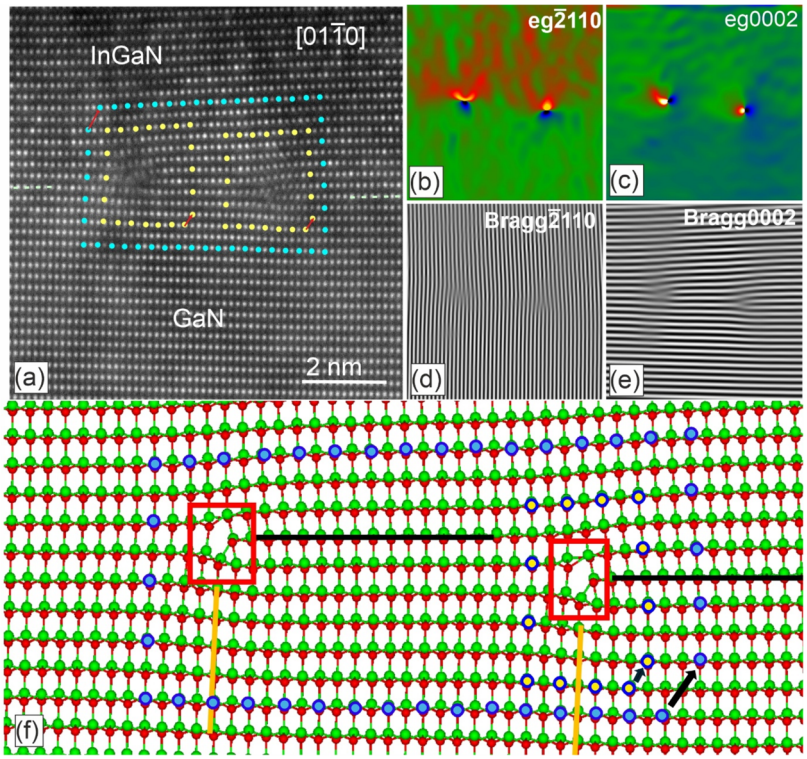

Figure 9. (a) HRSTEM image along the [01$\bar{1}$0] zone axis together with corresponding GPA maps showing in-plane (b) and out-of-plane (c) strain components of a dissociated **a** + **c** dislocation lying at the $In_{0.2}Ga_{0.8}N$/GaN interface, as well as Bragg filtered images (d, e) showing the extra half planes of the PDs. (f) Atomistic model of the dissociated dislocation in wurtzite GaN, shown along the dislocation lines, i.e., same zone axis as (a).

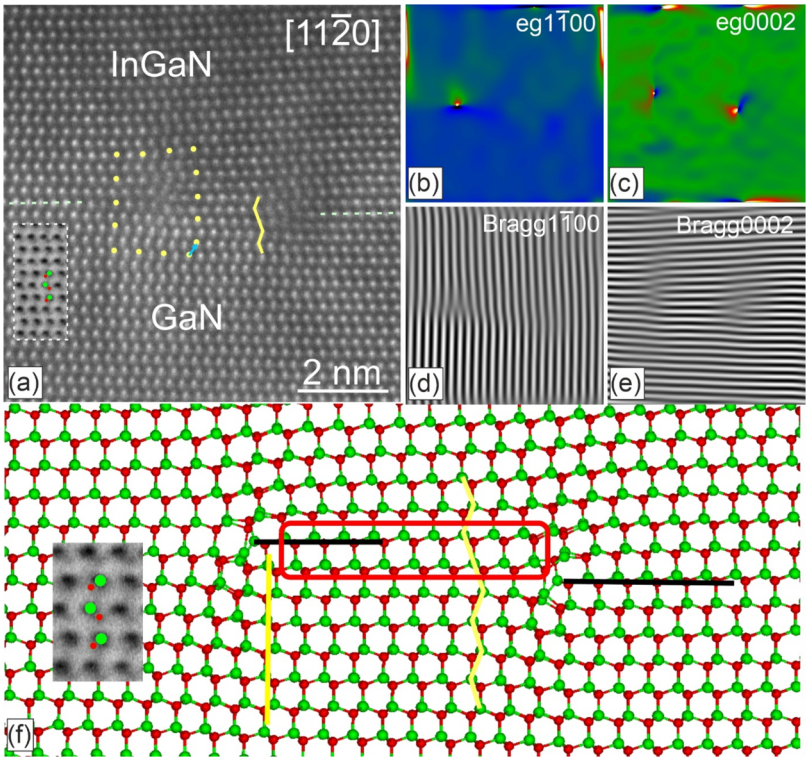

Figure 10. (a) HRSTEM image of the same defect as in Figure 9 (a) after 30° rotation to the [11$\bar{2}$0] zone axis, the I_1 BSF spreading between the two partial dislocations is well discernible. The inset in (a) is a BF-STEM image of GaN with indicated gallium and nitrogen atoms; (b, c) corresponding GPA maps showing in-plane (b) and out-of-plane (c) strain components of a dissociated **a** + **c** dislocation lying at the $In_{0.2}Ga_{0.8}N$/GaN interface, as well as Bragg filtered images (d, e) showing the extra half planes of the PDs. (f) Atomistic model of the dissociated dislocation corresponding to (a). Magnified part of the BF-STEM image is overlaid with the simulated structure, indicating the Ga-polarity of the GaN substrate and InGaN layer.

https://doi.org/10.1021/acsaelm.5c00859
ACS Appl. Electron. Mater. XXXX, XXX, XXX−XXX

half-plane associated with the **a**/2 component. The polarity of the core of the two partial dislocations was deduced from the polarity of the studied sample, which was grown with Ga polarity (insets in the Figure 10a,f).

In summary, the HRSTEM image (Figure 9a) represents a dissociated edge a + c dislocation into two 73° F−S PDs with either interstitial or vacancy core variants. The two resulting partials have a core configuration with a 3/5-atom ring structure, involving Ga−Ga bonds and N-dangling bonds, which characterizes a core with gallium polarity. The resulting atomistic configuration of the dissociated edge a + c dislocation is detailed in the models of Figures 9f and 10f.

5. DISCUSSION AND CONCLUSIONS

Atomistic simulations based on DFT were performed to investigate the atomic and electronic structures of F−S PDs with lines parallel to the *m*-direction in wurtzite GaN. The core configurations of the 55° and 73° partial dislocations with vacancy and interstitial structure variants and different polarities, gallium or nitrogen, were considered. A comprehensive procedure based on the mutual positions of the I_1 BSF and the extra half-plane associated with the **c**/2 edge component, was introduced to classify the core configurations into interstitial and vacancy variants.

The core configurations of the 55° PD were found to have a structure with a 7-atom ring, involving both Ga- and N-dangling bonds. These core configurations were associated with shallow gap states. The core configurations of the 73° PD, with gallium polarity, have a 3/5-atom ring structure involving Ga−Ga bonds and N-dangling bonds. However, those with nitrogen polarity exhibit a 6-atom ring structure involving both N- and Ga-dangling bonds. The core configurations of the 73° PD were associated with both shallow and deep gap states. The latter were found to be due to Ga−Ga bonds in the cores with gallium polarity and interacting N-dangling bonds in the cores with nitrogen polarity. According to the present results, the *m*-line Frank-Shockley and *a*-line Shockley PDs share the same origin of their associated deep gap states,[20] which are due to either Ga−Ga bonds or interacting dangling bonds. Such a generic-like feature needs to be further inspected for other dislocation types to assess its general character in wurtzite GaN. Our energetic calculations have demonstrated that the vacancy core configuration is the most energetically favorable for the 55° partial dislocation, whereas the interstitial ones are more favorable for both Ga and N polarities for the 73° partial dislocation.

The identification and discrimination between structural defects, such as dislocations, is a central problem in transmission electron microscopy imaging. In an edge-on observation, an F−S PD can be identified through its extra half-plane(s), associated with its edge component(s), its associated I_1 BSF, and the contrast produced by the core atoms in the observation plane. The more visible the latter elements, the easier it is to identify the PD.

In an edge-on observation, *a*-line F−S PDs are easier to identify than *m*-line ones, due to the visibility of their associated I_1 BSF.[21] The I1 BSF is not structurally visible along the <01$\bar{1}$0> zone axis, and a rotation of ± 30° around the *c*-axis is necessary to make it appear.[14] Distinguishing between the two *m*-line F−S PDs can be easily performed through identification of the extra half-planes associated with the different edge components. While the 73° partial dislocation has two such planes, the 55° has only one. A more difficult task would be a direct discrimination, i.e., without rotating the sample, between interstitial and vacancy core variants of the same *m*-line F−S PD. This is not the case for an *a*-line PD where the I_1 BSF and the extra half-planes are both visible in an edge-on observation.[21] Then, in the *m*-line F−S PD, a direct distinction between interstitial and vacancy core variants depends only on the projected structure of each core on the observation plane. Our structural calculations demonstrated that both core variants induce deformations with almost the same magnitudes (Table 1) and thus will be indistinguishable in edge-on observation. Resolving the Ga−N dumbbells in GaN is a much greater challenge in the *m*-direction than in the *a*- and *c*-directions, even with annular bright field HRSTEM imaging, due to the vertical separation of the two elements of just 0.6−0.7 Å along the *c*-axis.[45,46] This makes it impossible to directly discriminate between the interstitial and vacancy core variants of an *m*-line F−S PD in edge-on observation. Furthermore, our calculations demonstrate that the interstitial and vacancy core variants of an *m*-line F−S PD have identical electronic structures. This also makes it impossible to discriminate between them using experimental techniques that rely on the electronic structure, such as spatially resolved Electron Energy Loss Spectroscopy (EELS).[47,48]

Our structural analysis of the *m*-line F−S PD allowed for the elucidation of the dissociation of the **a** + **c** edge dislocation. Such dissociation is important because it allows for the relaxation of the interfacial stress between InGaN and GaN epilayers.[43,44] A dissociated **a** + **c** edge dislocation at the $In_{0.2}Ga_{0.8}N$/GaN interface was observed by HRSTEM. The **a** + **c** edge dislocation dissociates into two 73° *m*-line F−S PDs with the same polarity (Ga or N). It involves PDs with both interstitial and vacancy core variants. Moreover, our present results are a prerequisite to elucidate the structure of the m-line Shockley-like PDs surrounding I4 BSF domains. The latter domains, which are formed by the overlapping of two I1 BSFs with parallel-oriented zinc-blende structural units, have been proven to be sources of *a*-type threading dislocations.[8,25] This elucidation will constitute an important step toward rationalizing the mechanism of the nucleation of threading dislocations from BSF domains in III-nitride semiconductors.

AUTHOR INFORMATION

Corresponding Author

Julita Smalc-Koziorowska − *Institute of High Pressure Physics, Polish Academy of Sciences, Warsaw 01-142, Poland;* orcid.org/0000-0002-1460-7861; Email: julita@unipress.waw.pl

Authors

Imad Belabbas − *Université de Bejaia, Faculté des Sciences Exactes, Laboratoire de Physico-Chimie des Matériaux et Catalyse, Bejaia 06000, Algeria;* orcid.org/0000-0001-9200-0339

Joanna Moneta − *Institute of High Pressure Physics, Polish Academy of Sciences, Warsaw 01-142, Poland;* orcid.org/0000-0002-2748-7416

George P. Dimitrakopulos − *Department of Physics, Aristotle University of Thessaloniki, Thessaloniki GR-54124, Greece;* orcid.org/0000-0001-8499-2198

Joseph Kioseoglou − *Department of Physics, Aristotle University of Thessaloniki, Thessaloniki GR-54124, Greece; Center for Interdisciplinary Research and Innovation,*

https://doi.org/10.1021/acsaelm.5c00859
ACS Appl. Electron. Mater. XXXX, XXX, XXX−XXX

Aristotle University of Thessaloniki, Thessaloniki GR-57001, Greece; orcid.org/0000-0002-6933-2674

Jun Chen − *CIMAP-Alençon, UMR6252, CNRS-CEA-ENSICAEN, Université de Caen Normandie, Caen F-14032, France*

Witold Chromiński − *Faculty of Materials Science and Engineering, Warsaw University of Technology, Warsaw 02-507, Poland*

Complete contact information is available at: https://pubs.acs.org/10.1021/acsaelm.5c00859

Notes

The authors declare no competing financial interest.

■ ACKNOWLEDGMENTS

This work was funded in part by National Science Center, Poland, project OPUS LAP 2020/39/I/ST5/03379 and by Deutsche Forschungsgemeinschaft, Germany, project 465219948, and in part by National Science Centre, Poland, project Miniature 2024/08/X/ST11/00274. I. Belabbas acknowledges the University of Bejaia and the Algerian Ministry of High Education and Scientific Research for funding. The CRIANN (Centre Régional Informatique et d'Applications Numériques de Normandie, www.criann.fr) is acknowledged for providing computational resources. P R Briddon and M J Rayson from the University of Newcastle (UK) are acknowledged for providing access to the AIMPRO code.

■ REFERENCES

(1) Li, G.; Zhu, M.; Guo, Z.; Yang, Y.; Li, H.; Shang, J.; Feng, Y.; Lu, Y.; Gao, F.; Li, S. Recent Advances in III−V Nitrides: Properties, Applications and Perspectives. *J. Mater. Chem. C* **2024**, *12* (32), 12150−12178.

(2) Zhou, C.; Ghods, A.; Saravade, V. G.; Patel, P. V.; Yunghans, K. L.; Ferguson, C.; Feng, Y.; Kucukgok, B.; Lu, N.; Ferguson, I. T. Review—The Current and Emerging Applications of the III-Nitrides. *ECS J. Solid State Sci. Technol.* **2017**, *6* (12), Q149−Q156.

(3) Jain, S. C.; Willander, M.; Narayan, J.; Overstraeten, R. V. III−Nitrides: Growth, Characterization, and Properties. *J. Appl. Phys.* **2000**, *87* (3), 965−1006.

(4) Zakharov, D. N.; Liliental-Weber, Z.; Wagner, B.; Reitmeier, Z. J.; Preble, E. A.; Davis, R. F. Structural TEM Study of Nonpolar a -Plane Gallium Nitride Grown on (11 2¯ 0) 4 H -SiC by Organometallic Vapor Phase Epitaxy. *Phys. Rev. B* **2005**, *71* (23), No. 235334.

(5) Liliental-Weber, Z. Structural Defects in GaN Revealed by Transmission Electron Microscopy. *Jpn. J. Appl. Phys.* **2014**, *53* (10), No. 100205.

(6) Lähnemann, J.; Jahn, U.; Brandt, O.; Flissikowski, T.; Dogan, P.; Grahn, H. T. Luminescence Associated with Stacking Faults in GaN. *J. Phys. D: Appl. Phys.* **2014**, *47* (42), No. 423001.

(7) Stampfl, C.; Van De Walle, C. G. Energetics and Electronic Structure of Stacking Faults in AlN, GaN, and InN. *Phys. Rev. B* **1998**, *57* (24), No. R15052.

(8) Smalc-Koziorowska, J.; Moneta, J.; Chatzopoulou, P.; Vasileiadis, I. G.; Bazioti, C.; Prytz, Ø.; Belabbas, I.; Komninou, P.; Dimitrakopulos, G. P. The Heterogeneous Nucleation of Threading Dislocations on Partial Dislocations in III-Nitride Epilayers. *Sci. Rep.* **2020**, *10* (1), No. 17371.

(9) Belabbas, I.; Ruterana, P.; Chen, J.; Nouet, G. The Atomic and Electronic Structure of Dislocations in Ga-Based Nitride Semiconductors. *Philos. Mag.* **2006**, *86* (15), 2241−2269.

(10) Moram, M. A.; Ghedia, C. S.; Rao, D. V. S.; Barnard, J. S.; Zhang, Y.; Kappers, M. J.; Humphreys, C. J. On the Origin of Threading Dislocations in GaN Films. *J. Appl. Phys.* **2009**, *106* (7), No. 073513.

(11) Moustakas, T. D. The Role of Extended Defects on the Performance of Optoelectronic Devices in Nitride Semiconductors. *Phys. Status Solidi A* **2013**, *210* (1), 169−174.

(12) Narita, T.; Kanechika, M.; Kojima, J.; Watanabe, H.; Kondo, T.; Uesugi, T.; Yamaguchi, S.; Kimoto, Y.; Tomita, K.; Nagasato, Y.; Ikeda, S.; Kosaki, M.; Oka, T.; Suda, J. Identification of Type of Threading Dislocation Causing Reverse Leakage in GaN p−n Junctions after Continuous Forward Current Stress. *Sci. Rep.* **2022**, *12* (1), No. 1458.

(13) Wu, F.; Tyagi, A.; Young, E. C.; Romanov, A. E.; Fujito, K.; DenBaars, S. P.; Nakamura, S.; Speck, J. S. Misfit Dislocation Formation at Heterointerfaces in (Al,In)GaN Heteroepitaxial Layers Grown on Semipolar Free-Standing GaN Substrates. *J. Appl. Phys.* **2011**, *109* (3), No. 033505.

(14) Smalc-Koziorowska, J.; Moneta, J.; Muzioł, G.; Chromiński, W.; Kernke, R.; Albrecht, M.; Schulz, T.; Belabbas, I. The Dissociation of (A + c) Misfit Dislocations at the InGaN/GaN Interface. *J. Microsc.* **2024**, *293* (3), 146−152.

(15) Matthews, J. W.; Blakeslee, A. E. Defects in Epitaxial Multilayers. *J. Cryst. Growth* **1974**, *27*, 118−125.

(16) Komninou, Ph.; Kioseoglou, J.; Dimitrakopulos, G. P.; Kehagias, Th.; Karakostas, Th. Partial Dislocations in Wurtzite GaN. *Phys. Status Solidi A* **2005**, *202* (15), 2888−2899.

(17) Osipyan, Y. A.; Smirnova, I. S. Partial Dislocations in the Wurtzite Lattice. *J. Phys. Chem. Solids* **1971**, *32* (7), 1521−1530.

(18) Vasileiadis, I. G.; Belabbas, I.; Bazioti, C.; Smalc-Koziorowska, J.; Komninou, P.; Dimitrakopulos, G. P. Stacking Fault Manifolds and Structural Configurations of Partial Dislocations in InGaN Epilayers. *Phys. Status Solidi (b)* **2021**, *258* (11), No. 2100190.

(19) Belabbas, I.; Dimitrakopulos, G.; Kioseoglou, J.; Béré, A.; Chen, J.; Komninou, Ph.; Ruterana, P.; Nouet, G. Energetics of the 30∘ Shockley Partial Dislocation in Wurtzite GaN. *Superlattices Microstruct.* **2006**, *40* (4−6), 458−463.

(20) Belabbas, I.; Dimitrakopulos, G. P.; Kioseoglou, J.; Chen, J.; Smalc-Koziorowska, J. First-Principles Investigation of a-Line Shockley Partial Dislocations in Wurtzite GaN: Core Reconstruction and Electronic Structure. *Modell. Simul. Mater. Sci. Eng.* **2022**, *30* (8), No. 085004.

(21) Kioseoglou, J.; Dimitrakopulos, G.; Komninou, Ph.; Karakostas, Th. Atomic Structures and Energies of Partial Dislocations in Wurtzite GaN. *Phys. Rev. B* **2004**, *70* (3), No. 035309.

(22) Kioseoglou, J.; Kalesaki, E.; Lymperakis, L.; Neugebauer, J.; Komninou, Ph.; Karakostas, Th. Electronic Structure of 1/6 ⟨20$\bar{2}$3⟩ Partial Dislocations in Wurtzite GaN. *J. Appl. Phys.* **2011**, *109* (8), No. 083511.

(23) Giaremis, S.; Komninou, Ph.; Belabbas, I.; Chen, J.; Kioseoglou, J. Structural and Electronic Properties of *a* -Edge Dislocations along ⟨1−100⟩ in GaN. *J. Appl. Phys.* **2018**, *123* (24), No. 244301.

(24) Chen, C.; Meng, F.; Song, J. Core Structures Analyses of (a + c)-Edge Dislocations in Wurtzite GaN through Atomistic Simulations and Peierls−Nabarro Model. *J. Appl. Phys.* **2015**, *117* (19), No. 194301.

(25) Smalc-Koziorowska, J.; Bazioti, C.; Albrecht, M.; Dimitrakopulos, G. P. Stacking Fault Domains as Sources of A-Type Threading Dislocations in III-Nitride Heterostructures. *Appl. Phys. Lett.* **2016**, *108* (5), No. 051901.

(26) Moneta, J.; Siekacz, M.; Grzanka, E.; Schulz, T.; Markurt, T.; Albrecht, M.; Smalc-Koziorowska, J. Peculiarities of Plastic Relaxation of (0001) InGaN Epilayers and Their Consequences for Pseudo-Substrate Application. *Appl. Phys. Lett.* **2018**, *113* (3), No. 031904.

(27) Pristovsek, M.; Frentrup, M.; Zhu, T.; Kusch, G.; Humphreys, C. J. X-Ray Characterisation of the Basal Stacking Fault Densities of (11$\bar{2}$2) GaN. *CrystEngComm* **2021**, *23* (35), 6059−6069.

(28) Belabbas, I.; Belkhir, M. A.; Lee, Y. H.; Chen, J.; Béré, A.; Ruterana, P.; Nouet, G. Local Electronic Structure of Threading Screw Dislocation in Wurtzite GaN. *Comput. Mater. Sci.* **2006**, *37* (3), 410−416.

(29) Belabbas, I.; Nouet, G.; Komninou, Ph. Atomic Core Configurations of the -Screw Basal Dislocation in Wurtzite GaN. *J. Cryst. Growth* **2007**, *300* (1), 212−216.
(30) Béré, A.; Serra, A. On the Atomic Structures, Mobility and Interactions of Extended Defects in GaN: Dislocations, Tilt and Twin Boundaries. *Philos. Mag.* **2006**, *86* (15), 2159−2192.
(31) Press, W. H.; Teukolsky, S. A.; Vetterling, W. T.; Flannery, B. P. *Numerical Recipes in C: The Art of Scientific Computing*, 2nd ed.; Cambridge University Press: Cambridge, 1992.
(32) Hohenberg, P.; Kohn, W. Inhomogeneous Electron Gas. *Phys. Rev.* **1964**, *136* (3B), No. B864.
(33) Kohn, W.; Sham, L. J. Self-Consistent Equations Including Exchange and Correlation Effects. *Phys. Rev.* **1965**, *140* (4A), No. A1133.
(34) Briddon, P. R.; Jones, R. LDA Calculations Using a Basis of Gaussian Orbitals. *Phys. Status Solidi (b)* **2000**, *217* (1), 131−171.
(35) Hartwigsen, C.; Goedecker, S.; Hutter, J. Relativistic Separable Dual-Space Gaussian Pseudopotentials from H to Rn. *Phys. Rev. B* **1998**, *58* (7), No. 3641.
(36) Perdew, J. P.; Wang, Y. Accurate and Simple Analytic Representation of the Electron-Gas Correlation Energy. *Phys. Rev. B* **1992**, *45* (23), No. 13244.
(37) Monkhorst, H. J.; Pack, J. D. Special Points for Brillouin-Zone Integrations. *Phys. Rev. B* **1976**, *13* (12), No. 5188.
(38) Methfessel, M.; Paxton, A. T. High-Precision Sampling for Brillouin-Zone Integration in Metals. *Phys. Rev. B* **1989**, *40* (6), No. 3616.
(39) Schulz, H.; Thiemann, K. H. Crystal Structure Refinement of AlN and GaN. *Solid State Commun.* **1977**, *23* (11), 815−819.
(40) Polian, A.; Grimsditch, M.; Grzegory, I. Elastic Constants of Gallium Nitride. *J. Appl. Phys.* **1996**, *79* (6), 3343−3344.
(41) Belabbas, I.; Chen, J.; Nouet, G. Electronic Structure and Metallization Effects at Threading Dislocation Cores in GaN. *Comput. Mater. Sci.* **2014**, *90*, 71−81.
(42) Hirth, J. P.; Lothe, J. *Theory of Dislocations*; Wiley, New York, 1982.
(43) Moneta, J.; Kryśko, M.; Domagala, J. Z.; Grzanka, E.; Muziol, G.; Siekacz, M.; Leszczyński, M.; Smalc-Koziorowska, J. Influence of GaN Substrate Miscut on the XRD Quantification of Plastic Relaxation in InGaN. *Acta Mater.* **2024**, *276*, No. 120082.
(44) Moneta, J.; Grzanka, E.; Turski, H.; Skierbiszewski, C.; Smalc-Koziorowska, J. Stacking Faults in Plastically Relaxed InGaN Epilayers. *Semicond. Sci. Technol.* **2020**, *35* (3), No. 034003.
(45) Zamani, R. R.; Arbiol, J. Understanding Semiconductor Nanostructures via Advanced Electron Microscopy and Spectroscopy. *Nanotechnology* **2019**, *30* (26), No. 262001.
(46) Roshko, A.; Brubaker, M. D.; Blanchard, P. T.; Bertness, K. A.; Harvey, T. E.; Geiss, R. H.; Levin, I. Comparison of Convergent Beam Electron Diffraction and Annular Bright Field Atomic Imaging for GaN Polarity Determination. *J. Mater. Res.* **2017**, *32* (5), 936−946.
(47) Fall, C. J.; Jones, R.; Briddon, P. R.; Blumenau, A. T.; Frauenheim, T.; Heggie, M. I. Influence of Dislocations on Electron Energy-Loss Spectra in Gallium Nitride. *Phys. Rev. B* **2002**, *65* (24), No. 245304.
(48) Yamashita, S.; Fukushima, S.; Kikkawa, J.; Arai, R.; Kanitani, Y.; Kimoto, K.; Kudo, Y. Local Defect and Mid-Gap State Analysis of GaN Using Monochromated EELS Combined with Nanodiffraction and Atomic-Resolution Imaging. *APL Mater.* **2024**, *12* (3), No. 031101.

https://doi.org/10.1021/acsaelm.5c00859
ACS Appl. Electron. Mater. XXXX, XXX, XXX−XXX